Communication

# Hybrid piezo/triboelectric nanogenerator for highly efficient and stable rotation energy harvesting

Chunlin Zhao[a,b,c,1], Qian Zhang[a,b,1], Wenliang Zhang[a], Xinyu Du[a], Yang Zhang[a], Shaobo Gong[a,b,c], Kailiang Ren[a,b], Qijun Sun[a,b,d], Zhong Lin Wang[a,b,d,e]

[a] Beijing Institute of Nanoenergy and Nanosystems, Chinese Academy of Sciences, Beijing 100083, China
[b] School of Nanoscience and Technology, University of Chinese Academy of Sciences, Beijing 100049, China
[c] Institute of Semiconductors, Chinese Academy of Sciences, Beijing 100083, China
[d] Center on Nanoenergy Research, School of Physical Science and Technology, Guangxi University, Nanning 530004, China
[e] School of Materials Science and Engineering, Georgia Institute of Technology, Atlanta, GA 30332-0245, United States

## ARTICLE INFO

## ABSTRACT

To develop highly efficient energy harvesting means to sustainably driving miniaturized portable electronic devices, the hybrid nanogenerators (NGs) are emerging to compensate for the respective shortcomings of either type of NG. However, the crucial factors affecting the output performances of hybrid NGs still exist, such as the driving frequency, phase difference and mismatched impedance. Here, the bimorph-based piezoelectric NG was integrated into the triboelectric NG to construct a hybrid piezo/triboelectric NG (H-P/TENG) for highly efficient mechanical rotation-energy harvesting. Systematic measurements and analyses illustrated the output performance of H-P/TENG was independent of the rotation speed (driving frequency) due to the invariable periodic deformation degree of the H-P/TENG. Both NGs in the H-P/TENG had the identical phase and matched impedance in the same magnitude, which were beneficial for direct coupling of their individual rectified output signals and avoided unnecessary energy loss from the utilization of transformer. Under a low rotation speed of 100 rpm, the proposed H-P/TENG delivered high output voltage, output current and large average power/power density at ~210 V, 395 µA and 10.88 mW/6.04 mW cm$^{-2}$, respectively. The output voltage/current of the sophisticated H-P/TENG could retain at ~210 V/400 µA under rotation speeds from 50 to 250 rpm. Through integrating an energy managing circuit with the H-P/TENG, we developed a DC power source (stable DC output at 3.6 V) to sustainably drive RF wireless temperature sensing network and commercial electronics. The H-P/TENG was also capable of producing high output voltage (150 V) and current (150 µA) at wind speed of 14 m/s to power 50 LEDs in parallel connection. The distinctive structure and outstanding performance of this hybrid NG is promising for the practical application of self-powered systems and the large-scale energy conversion.

## 1. Introduction

Energy crisis originated from exhausted resources, global warming induced by greenhouse effect, and the air pollution from imperfect combustion of fossil fuels are increasingly aggravated to diminish the quality of human life. Meanwhile, huge amount of sensors, portable electronics, wearable devices and wireless transport systems required in the coming era of Internet of Things bring about more concerns on the raising demands for energy supply [1–7]. Great efforts have been contributed to seek the clean energy harvesting means from renewable resources or ambient environments [8–13]. The triboelectric nanogenerator (TENG) has been extensively developed to scavenge widely distributed mechanical energy for the self-powered sensors or systems

[14–19]. According to the triboelectrification and electrostatic induction [17], the constant open-circuit voltage outputs of TENG under the threshold frequency range (< 5 Hz) is promising to harvest abundant mechanical energies at low frequency [20–22], such as breathing, walking [23], arm swing [24], human motions [25], rain dropping [26], wind/water flow [27], ocean wave [28], *etc.* However, the extremely large internal resistance in TENG inevitably leads to a limited output current, which directly pulls down the total output power and energy conversion efficiency [29–32]. Strategies for boosting the output power of TENG have never been stopped through increasing the surface roughness, introducing electric double layers, or creating hysteretic ferroelectric polarization [33–37]. More versatile and practical methods are still eagerly encouraged to launch for improving the

---

energy conversion efficiency of TENG.

The hybridization of different types of NGs offers an efficient approach to enhancing the output powers by simultaneously harvesting multiple types of energy [38–40]. The integration of TENG with electromagnetic generator (EMG) is promising to cover the shortage of the inefficient energy harvesting capacity of EMG at low mechanical frequency [29,30]. Introducing pyroelectric materials into TNEG is reasonable to harvest the thermal energy from ambient environment or even the friction-induced temperature increment [38,41]. Compared with other types of NGs, the piezoelectric nanogenerator (PENG) is capable of delivering high conversion efficiency and stable output powers under weak and low frequency mechanical stimuli [42–44]. The intrinsic thin-film nature of the active layers in both TENG and PENG allows the facile integration into desired structures for specific applications. The matching of the impedance between PENG and TENG is easier to adjust due to the broad selection of various piezoelectric polymers/composites/nanofibers, which promises to desuetude the transformer to avoid extra energy loss. Generally, the PENG exhibits the optimal energy conversion efficiency at the resonant states due to the matched resonance frequency between the piezoelectric component and external mechanical sources [45–47]. Thereby, how to effectively hybridize the PENG and TENG by activation of the resonance mode and diminishing the output phase differences is urgently demanded to realize efficient and stable mechanical energy harvesting.

In this work, we developed a high performance hybrid piezo/triboelectric NG (H-P/TENG) by integrating a bimorph-based PENG into a one-end-fixed TENG. The fabricated H-P/TENGs were mounted on three upright posts of a custom frame ("stator") and subjected to bending strains from a coaxial tri-blade structure ("rotor") to harvest rotary mechanical energy. The working mechanism of H-P/TENG combined with time dependent output phase analysis was investigated in details. The rectified output signals of both NGs were collected in parallel mode, Under the synergistic effect of triboelectrification and piezopolarization, the H-P/TENG could deliver high open-circuit voltage (210 V), short-circuit current (395 μA), large average output power (10.88 mW) and power density (6.04 mW/cm$^2$) due to the integration of high performance bimorph-based PENG and their matched impedances. Notably, the output performances of H-P/TENG retained stable with rotation speed ranged from 50 to 250 rpm due to the invariable periodic deformation degree of the H-P/TENG. The proposed hybrid NG showed highly efficient performance to drive 50 parallel LEDs and charge a capacitor (47 μF). Moreover, according to the stable output characteristics, we developed an individualized energy managing circuit for the H-P/TENG to supply a stable constant output voltage (3.6 V) for sustainably driving diverse commercial electronics (*e.g.* radio-frequency wireless transport system, temperature sensor, calculator, *etc.*). The H-P/TENG was also capable of harvesting wind energy for practical application. At a wind speed of 14 m/s, high output voltage (150 V) and current (150 μA) were attained for driving 50 LEDs. The proposed H-P/TENG exhibited excellent capacity in harvesting broadband mechanical energy independent of driving frequency, which is highly promising to harvest mechanical energy in arbitrary modes (*e.g.* periodic bending, vibration, rotation, *etc.)* for sustainable portable electronics, sophisticated wearable devices, and self-powered systems.

## 2. Results and discussion

Fig. 1**a** shows the schematic illustration of the H-P/TENG mounted in the custom frame for harvesting rotary mechanical energy. Three H-P/TENGs were mounted on three upright posts in the frame as the "stator", while a rotatable axle with acrylic blades acted as the "rotator". Three wind cups were added to the top of rotatable axle to harvest wind energy. The structure image of H-P/TENG is enlarged in the inset of Fig. 1**a**. A bimorph structured PENG was utilized, which consisted of two layers of poly(vinylidenefluoride-*co*-trifluoroethylene) (P(VDF-TrFE)) sandwiched between three layers of Au electrodes. Then

the PENG was integrated into the base layer of a one-end-fixed TENG constructed with polyethylene terephthalate/Al (PET/Al) and polytetrafluoroethylene/Au (PTFE/Au) layer in contact-separation mode. When the H-P/TENG was subjected to the "rotator" blade, equivalent contact-separation process and external strain were applied to the hybrid device. Thus, the rotary mechanical energy could be converted into electricity. The fabrication process of the H-P/TENG is shown in the left panel of Fig. 1**b** (right panel is the photo image). In order to achieve high output performance from H-P/TENG, P(VDF-TrFE) film with a preferential ferroelectric β-phase was utilized as the piezoelectric layer. The copolymerization of VDF and TrFE monomers induced an all-trans conformation due to the increased steric hindrance by the third fluoride in TrFE, which facilitated the formation of the piezoelectric β-phase [48,49]. As demonstrated in Fig. S1a, the diffraction peak at 20° in the X-ray pattern suggested the dominant β-phase in the annealed P(VDF-TrFE). The typical needle-like crystalline domains of the P(VDF-TrFE) was observed by scanning electron microscopy (Fig. S1b). The bimorph-based PENG was introduced with two P(VDF-TrFE) films connected in parallel as shown in Fig. S2a (the equivalent circuit in Fig. S2b). According to Fig. S2a, the bending deformation of the PET substrate in the H-P/TENG was induced when the blade swept the H-P/TENG. Meantime, the film-1and film-2 was subjected to the tension and compression stress, respectively. The output voltage and current of the bimorph-based PENG was 72 V and 500 μA, respectively (Fig. 1**c** and **d**), the enlarged images of single peak from the short-circuit current and open-circuit voltage were illustrated in Fig. S2c and S2d. It was observed that the output current of bimorph-based PENG was twice higher than the unimorph-based PENG, but the output voltage was equal to each other (Fig. S3c and S3d). Therefore, the bimorph-based PENG with superior performance was able to compensate the shortcomings of low current output in TENG and greatly improve the output power of the hybrid NGs by efficiently harvesting mechanical energy. Besides, the utilization of bimorph structure in H-P/TENG was an effective way to broadening the resonance frequency range of piezoelectric part by matching with variable vibration frequency during the rotation stimuli, so as to maximize the total energy conversion efficient. For TENG part, the evenly distributed nanodots were introduced on the surface of PTFE through inductively coupled plasma (ICP) etching process to increase the active points for effective triboelectrification (Fig. S1c) [50]. The poling process was also utilized to inject negative charges onto the surface of the PTFE film to enhance the surface charge density and confine an inner polarized electric field.

The operation process and charge transfer mechanism of the H-P/TENG are detailedly illustrated in Fig. 2**a**. To comprehend the working principle of H-P/TENG clearly, we conducted synchronous measurements on the individual NG in the hybrid device to check the corresponding output signal simultaneously. Each part of the output signal is distributed to the related operating process as marked in Fig. 2**b**. At the initial state (Fig. 2**a** (i)), the rotor blade did not contact the PET/Al sheet. Neither piezoelectric nor triboelectric potential was generated because two friction layers did not contact each other and no bending deformation existed in the PET substrate. Further rotation would force the tilted PET/Al to continuously approach the PTFE surface (Fig. 2**a** (ii)). Under the combination of the electrostatic induction and triboelectrification, the accumulated opposite charges on Al/PTFE surface tended to be neutralized during approaching, which attracted compensated charges from Al/Au electrodes through external load. This process resulted in an output voltage in TENG. As the axle continued to rotate until the Al electrode got into full contact with PTFE film (Fig. 2**a** (iii)), the induced electrostatic charges on metal electrodes /PTFE were balanced. The negative output voltage reached the maximum value (stage *ii* in red curve, Fig. 2**b**). Sustained rotation of the axle caused a further bending deformation on the fully contacted TENG, which delivered corresponding tensile stress to the bimorph structured PENG and induced a $d_{31}$ mode piezoelectric potential in P(VDF-TrFE) layers (Fig. 2**a** (iv)). The piezopotential attracted free electrons to balance the
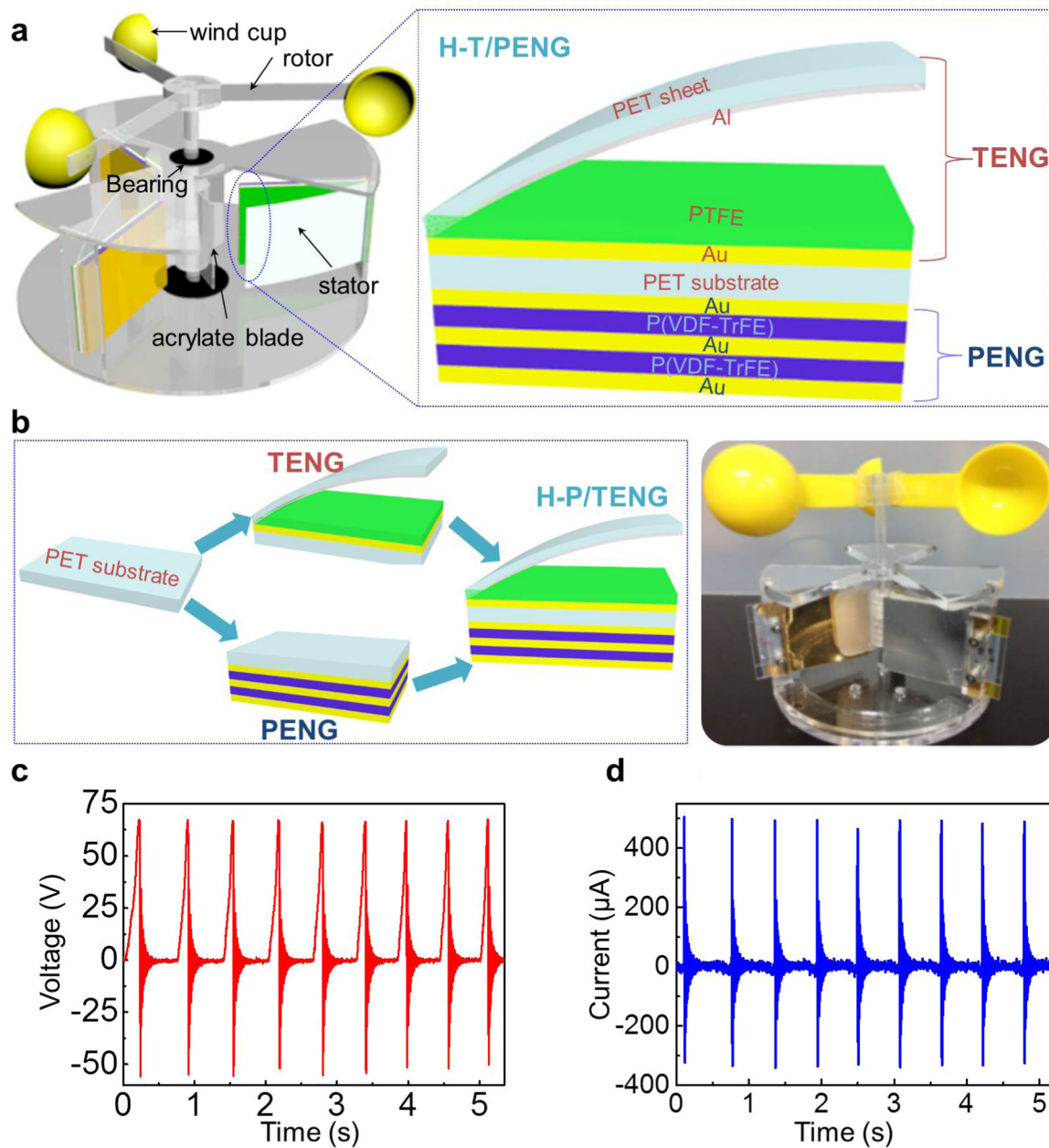
**Fig. 1.** (a) Schematic illustration of the H-P/TENGs mounted in the custom frame. Inset is the enlarged structure of single H-P/TENG. (b) Fabrication process of the H-P/TENG. Right panel is the photo image of the fabricated device for harvesting rotary mechanical energy. (c) (d) The open-circuit voltage and short-circuit current of the bimorph-based PENG.

induced polarization charges through an external load, resulting in output voltage from PENG. When the H-P/TENG was subjected to the largest bending strain, the polarization charge density reached the maximum status, inducing the negative output voltage peak (stage *iv* in blue curve, Fig. 2**b**). During the further bending process of H-P/TENG after the full contact between PET/Al and PTFE, the observed turbulence output voltage (stage *iii* in red curve, Fig. 2**b**) might be attributed to the dislocation between PET/Al and PTFE during subjection to the acrylate blade. When the plastic blade was further rotate to exceed the free end of PENG, an instantaneous resilience occurred in H-P/TENG, causing a simultaneous process of strain recovery and Al/PTFE separation (Fig. 2**a** (v) and (vi)). The simultaneous resilience processes were further evidenced by the maximum positive output voltages of TENG and PENG in the identical phase (stage *v* in both red and blue curves, Fig. 2**b**). According to the hybrid structure design, the output voltages in the release process exhibited damping characteristics (stage

*vi*, Fig. 2**b**), which could contribute to the total outputs after individual rectifications. For the H-P/TENG, the PENG output lagged behind the TENG output due to the asynchronization between the maximum bending strain and full contact of PET/Al and PTFE. However, the output signals of TENG and PENG had the identical phase at the resilience point, which was beneficial for increasing the total output power. According to the above analysis, a highly efficient hybrid NG is predictable by integrating TENG and bimorph-based PENG with outputs in the identical phase. Further optimization of the frame geometry, device structure, and utilized materials may enable to achieve the identical phases in both of the outputs (positive and negative output peaks) to maximize the total output power.

To evaluate the output characteristics of the H-P/TENG quantitatively, we mounted three H-P/TENGs to the frame and utilized a rotary motor to drive the rotor to impose the mechanical stimuli (at a low speed of 100 rpm). The TENG delivered high output voltage at 190 V
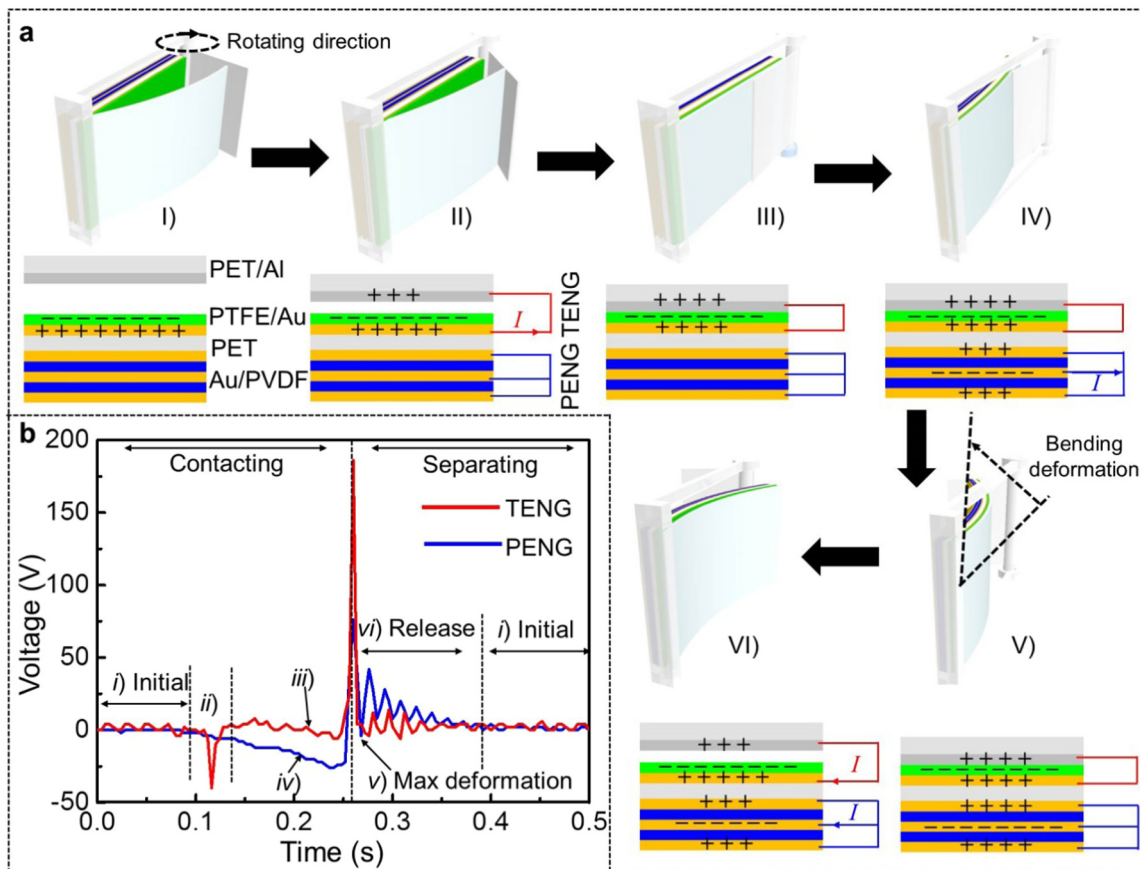
**Fig. 2.** (a) Schematic diagram of the working process and mechanism of the H-P/TENG, the black arrow indicate the rotation direction. The acrylic blade firstly contacts the PET sheet and later induces a bending deformation in PENG. (I) Initial state without any driving force, neither piezoelectric nor triboelectric potential exists. (II) The blade contacts the PET/Al layer and decreases the distance between the Al electrode and PTFE. The current occurs in TENG. (III) Continuous rotation of the rotor until PET/Al fully contact with PTFE. The induced charges are neutralized. (IV) The shaft continues to rotate and bends the PENG, which induces the $d_{31}$ piezoelectric potential and current output in PENG. (V) The PENG deformation reaches the maximum and induces the maximum piezoelectric potential. (VI) The acrylate blade sweeps through the free end of H-P/TENG and causes the resilience process, which results in a reverse current in both TENG and PENG. (b) Synchronous measurements on the output voltage of the individual NG in the hybrid device. Each part of the signal is attributed to the operating stage in Fig. 2a.

with low output current at 28 μA, as depicted in Fig. S4a and Fig. S4b. The frequency of the measured alternating current (AC) is 5 Hz, which is in accordance with the frequency extracted from the following equation:

$$f = \frac{nv}{60} \tag{1}$$

where $n$ is the number of H-P/TENGs and $v$ is the rotation speed (rpm). According to the identical periodic rotation between TENG and PENG, the frequency of the alternating piezoelectric current from PENG was also 5 Hz. The PENG exhibited much higher current of 375 μA with relatively lower voltage of 60 V (Fig. S4c and S4d). The output signals of both NGs had the identical phase when the blade swept through the H-P/TENG, which might have much higher current and voltage by combining the advantages of PENG and TENG.

To further avoid the partial counteractions of the individual output in the contact process and drastically exploit the output powers in the whole process, two independent full-wave diode bridges were connected to the PENG and TENG for rectification, respectively. To qualify the output performance of the hybrid NGs, the two rectification circuits were connected in parallel and characterized by Keithley 6514 (Fig. S5). The maximum rectified output voltage and current for the TENG were 190 V and 28 μA, respectively (Fig. 3a and b). A resistance box was connected in series with the rectification circuit to acquire the average power of the TENG. The current decreased with increased resistance and the average output power was obtained to be 1.95 mW at

the matching impedance of 10 MΩ (Fig. 3c). The rectified maximum voltage and current of PENG were characterized to be ~60 V and 400 μA, respectively (Fig. 3d and e). The PENG showed high output current with low output voltage, which was appropriately complementary with the TENG output performances. The average output power of PENG was extracted to be 8.67 mW at the matching impedance of ~1 MΩ (Fig. 3f). Based on the previous researches on the hybrid NG, it was generally to use transformers to adjust the matching impendence of both units to the same order of magnitude to avoid more energy loss. However, the coil heating would take away a large amount of the energy. For instance, the energy loss from TENG reached 86% through the coil in the transformer [29]. Moreover, the charging ability of hybrid NG was severely limited compared to any individual NG due to abnormal energy loss. In this paper, the matching impedances for both NGs were in the same order of magnitude, which allowed the direct connection of the rectified circuits without transformers to avoid the unwanted energy loss. Fig. 3g and h describe the output voltage and current of H-P/TENG, respectively. The output voltage of H-P/TENG was slightly higher (~200 V) than that of TENG, and the output current (~400 μA) was similar with PENG. The H-P/TENG inherited the merits of both types of NGs (*i.e.* high output voltage and current). The average output power was estimated to be 10.88 mW with the matching impedance of ~1 MΩ (Fig. 3i), which was slightly larger than the sum of the output powers of individual NG. The main reasons for the superior output performance of H-P/TENG are attributed to: (i) the rectified signals of both NGs have the identical phase; (ii) the matching impedances for
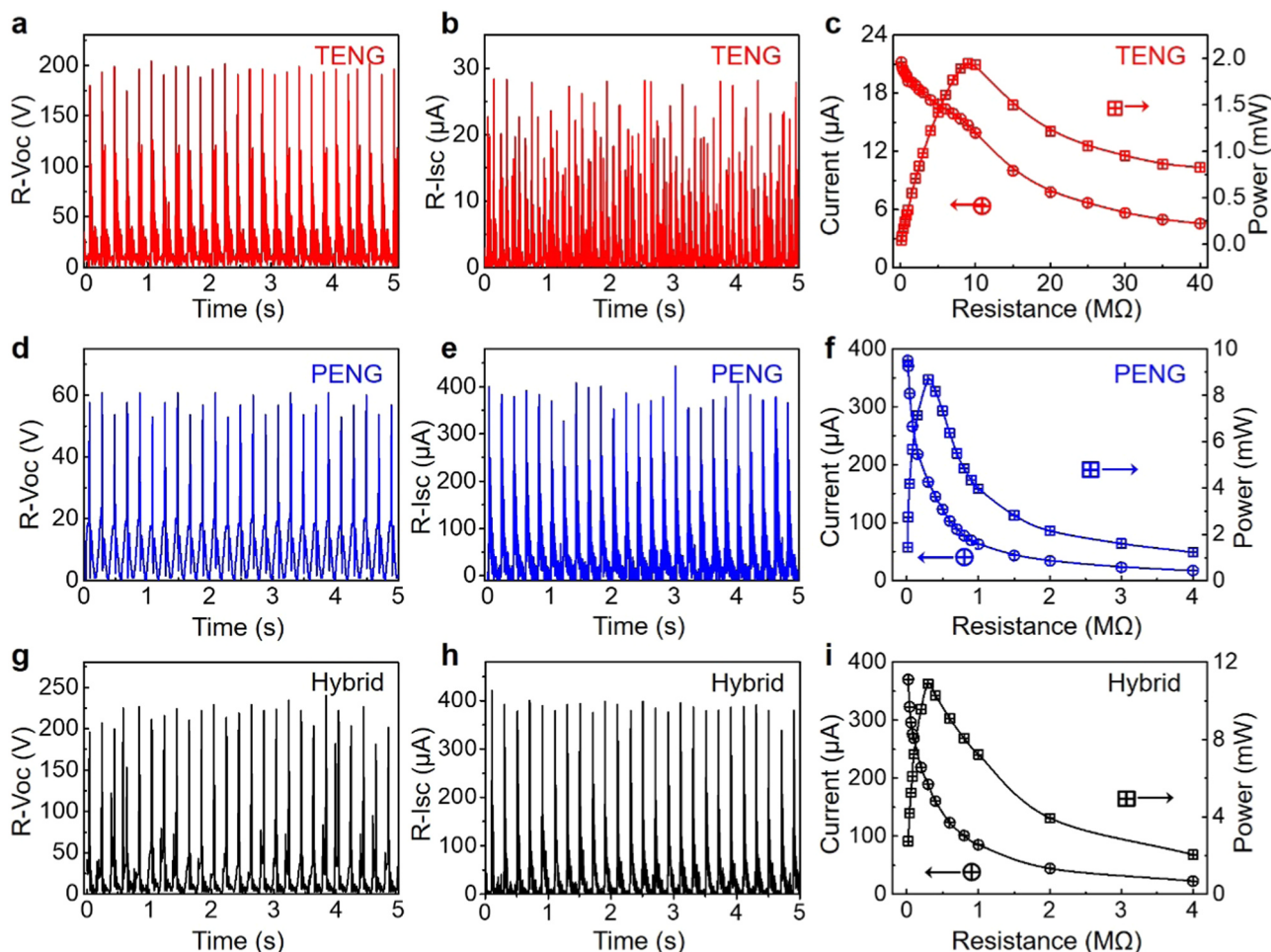
**Fig. 3.** Electrical output properties of the rectified TENG, PENG and H-P/TENG with a rotation speed at 100 rpm. (a) (b) Rectified open-circuit voltage and short-circuit current of TENG. (c) Dependence of output current and average power of the TENG on the external loading resistance. (d) (e) Rectified open-circuit voltage and short-circuit current of PENG. (f) Output current and average power of PENG *vs.* external loading resistance. (g) (h) Output open-circuit voltage and short-circuit current of H-T/PTENG. (i) The relationship between output current/average power of H-P/TENG and external loading resistance.

output powers are in the same magnitude; (iii) the parallel connection of the rectified both NGs may reduce the overall internal resistance of the H-P/TENG. Hence, the proposed H-P/TENG is anticipated to be a desirable device for highly efficient energy harvesting.

To further investigate the properties of H-P/TENG, the systematic measurements and theoretical analyses related with rotation speed (working frequency), adopted substrate modulus, and resonance frequency of PENG were conducted. With different rotation speeds ranging from 50 to 250 rpm, all the rectified open-circuit voltages of the TENG, PENG and H-P/TENG remained unchanged (Fig. 4a). In contrast, the rectified short-circuit currents of the TENG increased from 28 to 40 μA with increased rotation speed, while the output currents for PENG were nearly unaffected by the rotation speeds (maintained at ~390 μA). For the H-P/TENG, the output current showed a similar variation trend with TENG (increased from 415 to 435 μA with increased rotation speed), mainly determined by the variable output currents of TENG under different speeds (Fig. 4b).

Theoretical analyses were carried out to interpret the measured results above. Based on Gauss theorem, the voltage of TENG ($V_{OC}$) is described by [51,52]:

$$V_{OC} = -\frac{Q}{S\varepsilon_0}\left(\frac{d}{\varepsilon_1} + x\right) + \frac{\sigma x}{\varepsilon_0} \tag{2}$$

where $Q$ is the amount of transferred charges between two electrodes during electrostatic induction, $x$ is the distance between two friction

layers, $d$, $\sigma$, $S$, $\varepsilon_1$, and $\varepsilon_0$ are the friction layer thickness, surface charge density, electrode area, dielectric constant of the PTFE and the permittivity of vacuum, respectively. From Eq. (2), the voltage for TENG is mainly determined by the amount of transferred charges and surface charge density. The variables ($d$ and $\sigma$) in Eq. (2) are irrelevant to the rotation speed, resulting in the $V_{OC}$ of TENG remains constant at any rotation speed. The current density for the TENG ($J_D$) is explained by [53]:

$$J_D = \sigma\frac{dx}{dt}\frac{\frac{d\varepsilon_0}{\varepsilon_1} + \frac{d_2\varepsilon_0}{\varepsilon_2}}{\left(\frac{d\varepsilon_0}{\varepsilon_1} + \frac{d_2\varepsilon_0}{\varepsilon_2} + x\right)^2} \tag{3}$$

where the $\sigma$, $x$, $\varepsilon_1$, $d$, and $\varepsilon_0$ have the same physical meaning with Eq. (2). $d_2$, and $\varepsilon_2$ are the thickness and dielectric constant of the other friction layer, respectively. Obviously, the displacement current density ($J_D$) is proportional to the surface charge density ($\sigma$) and the separation speed ($\frac{dx}{dt}$) of two friction layers. Accordingly, the TENG output current increased with the increased rotation speed. For the PENG, its output voltage and current were proportional to the tensile strain applied to the P(VDF-TrFE) film, which was determined by the length of acrylic blade on the axle and independent of rotation speed. Therefore, the output signals of the PENG did not change with the rotation speed. To interpret the frequency dependent performance of the H-P/TENG (stable voltage and varied current outputs at different rotation speeds), the rectified voltages of both TENG and PENG were simultaneously
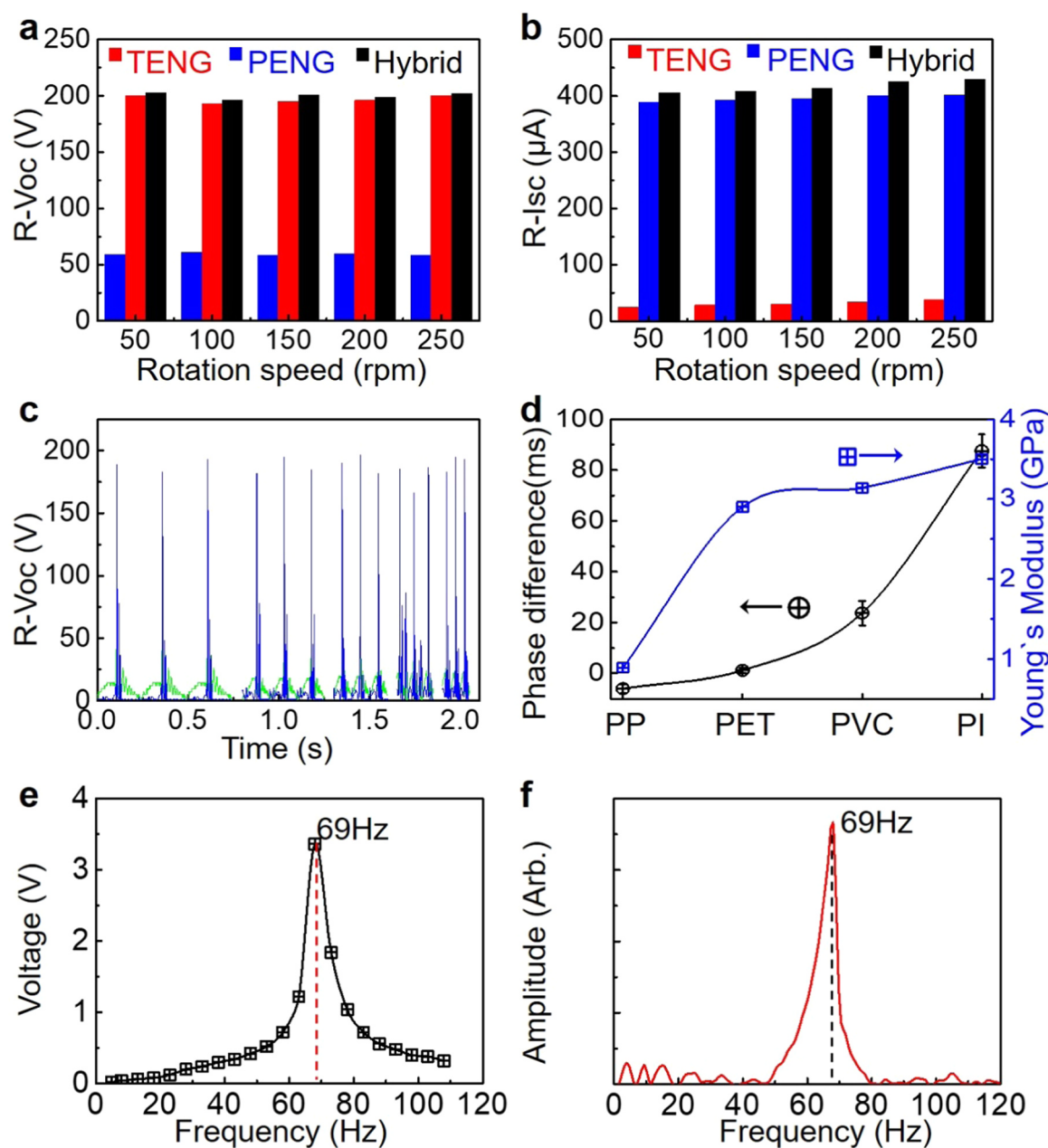
**Fig. 4.** (a) (b) The rectified open-circuit voltage and short-circuit current of TENG, PENG and H-P/TENG at rotation speeds from 50 rpm to 250 rpm. (c) The synchronous rectified open-circuit voltage of the PENG and TENG at rotation speeds from 50 rpm to 250 rpm. The corresponding enlarged views are Fig. S6. (d) The phase differences/Young's modulus *vs.* different substrates. (e) The open-circuit voltage of the PENG@PTFE/PET *vs.* the driving frequency of the shaker (1.2 m² s⁻¹). (f) Amplitude *vs.* frequency response obtained by Fast Fourier Transform for the energy dissipation spectrum of the PENG in Figure S7d.

characterized under different rotation speeds (Fig. 4c). All the rectified output voltages had the identical phase under varied rotation speeds (from 50 to 250 rpm, enlarged coordinates in Figure S6). According to the identical phase, it was applicable to superpose the frequency dependent TENG output current onto the invariable PENG output current to enhance the total output current of H-P/TENG. Meanwhile, the frequency dependence of H-P/TENG output current was attributed to the variable TENG output currents (*versus* the rotation speeds). Although the stable output voltage under different speeds slightly scarified the energy conversion efficiency, it represented great advantage for stably harvesting low-frequency and broadband mechanical energy.

In this work, the achieved identical output voltage phases during the resilience procedure of TENG, PENG and H-P/TENG close

correlated with the PET substrates. As the resilience was a dynamic mechanical process, the modulus of the selected substrates was critical to the NG output phases mainly determined by the recovery procedure. We defined the phase difference with the lag time between the individual output voltage of TENG and PENG. Commonly used substrates (*e.g.* polyimide (PI), polyvinyl chloride (PVC), polypropylene (PP), and PET) in the same thickness were selected to verify the relationship between the phase differences and Young's modulus. As shown in Fig. 4d, the phase difference increased with the increased Young's modulus of the substrate at a rotation speed of 100 rpm. Larger Young's modulus led to faster resilience speed, equivalent to applying relative large external force on the substrate to minimize (or eliminate) the phase differences of the outputs. Besides, the resonance theory of the

piezoelectric cantilever beam was introduced to explain the highly efficient mechanical energy scavenging by the H-P/TENG. To reproduce the effective model of H-P/TENG and simulate the bending process realistically, we prepared a bimorph-based PENG on PET/PTFE substrate (PENG@PET/PTFE, *i.e.* the H-P/TENG without PET/Al friction layer) and fixed it on the shaker with an accelerometer (testing setup in Figure S7a). The shaker was utilized to provide a sine incentive vibration with a sine acceleration of $1.5\,m^2\,s^{-1}$ (Figure S7b). The output voltages of PENG@PET/PTFE as a function of the driving frequency of testing setup are illustrated in Fig. 4e. The resonant frequency of PENG@PET/PTFE was 69 Hz, consistent with the frequency of the real-time sine output voltages (Figure S7c). Within one rotation cycle, the PENG underwent a typical damping vibration after the resilience, exhibiting a corresponding energy (or voltage) dissipation as shown in Figure S7d. Amplitude-frequency characteristic could be extracted from the energy dissipation spectrum through the fast Fourier transform (Fig. 4f) [54]. The achieved frequency (69 Hz) from the amplitude peak was the intrinsic resonant frequency of the bimorph-based PENG, which was in accordance with the resonant frequency of the PENG (69 Hz extracted from Figure S7c). Generally, the energy conversion efficiency of the piezoelectric cantilever beam reaches the maximum only at the resonant condition. Therefore, the PENG utilized in this work operated in the resonant condition at 69 Hz and attained the maximum energy conversion efficiency in the process of damping vibration. Thus, all the rotary mechanical energy imposed to the H-P/TENG could contribute to the output performance to enhance the efficiency of mechanical energy harvesting.

The H-P/TENG possesses both advantages of TENG (low frequency energy harvesting) and PENG (high output power), which is essential for efficiently powering electronics. As shown in Fig. 5a and b, the H-P/TENG was utilized to light up 50 LEDs in both series and parallel connections at a low rotation speed of 100 rpm (**Video s1** and **s2**). Single TENG upon the same rotation speed was also able to light up 50 LEDs in series and parallel. However, the brightness of LEDs was much darker (Figure S8a and S8b). The charging abilities of the TENG, PENG and H-P/TENG were verified by charging a capacitor of 47 μF at a fixed time, respectively (circuit diagram in Figure S8c). The highest charged voltage (11 V) for the capacitor was obtained by the H-P/TENG within 45 s (Fig. 5c). Obviously, the output performance and charging ability of the H-P/TENG were much better than that of either individual NG.

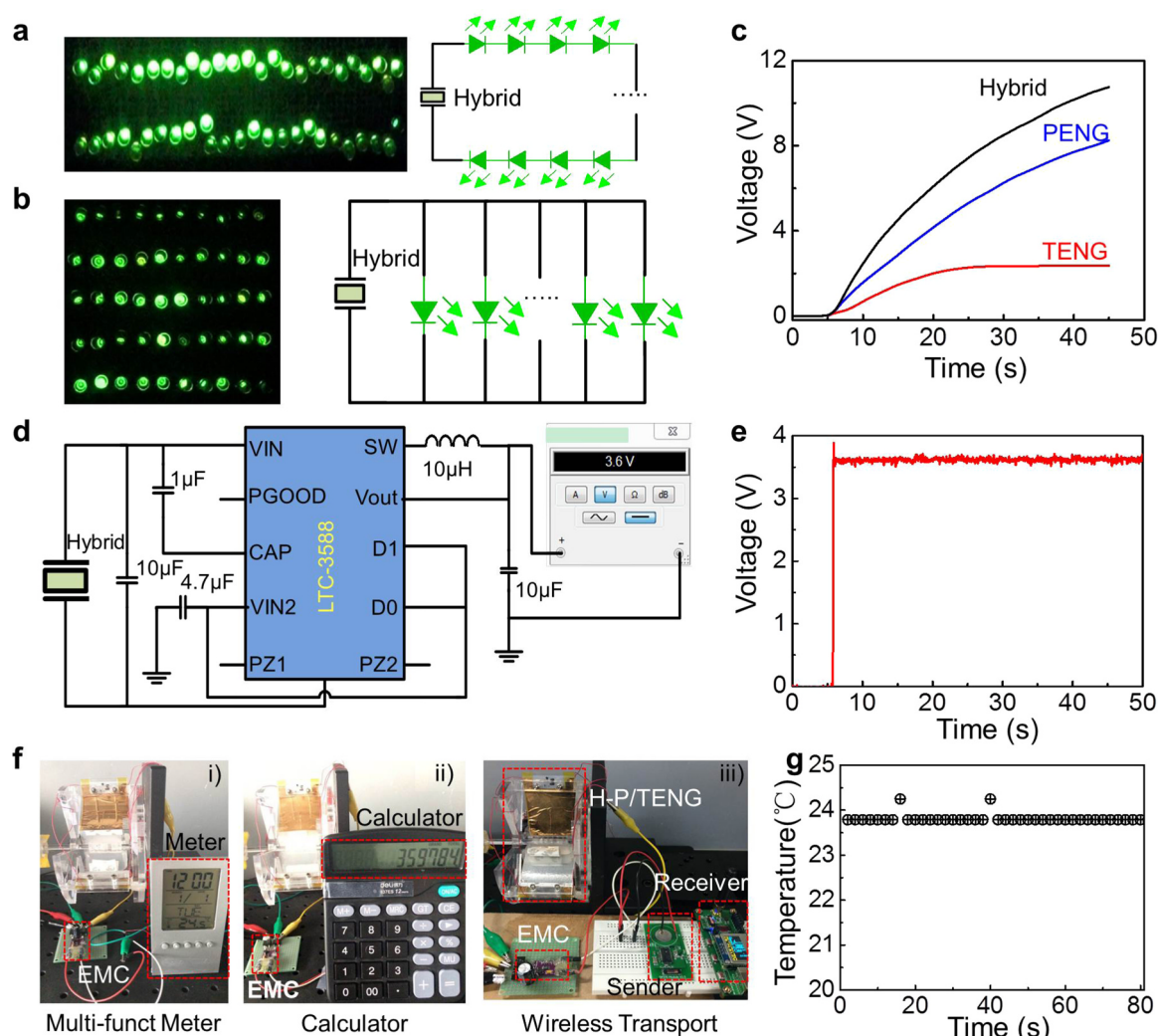Supplementary material related to this article can be found online at doi:10.1016/j.nanoen.2018.12.062.



**Fig. 5.** (a) (b) The photo image of 50 series and parallel LEDs driven by the H-P/TENG at rotation speed of 100 rpm. (c) 47 μF capacitor charging by the TENG, PENG and the H-P/TENG. (d) The circuit diagram of a complete DC power source with constant output voltage at 3.6 V. (e) Measured constant output voltage of DC power source. (f) The developed DC power source was utilized to drive diverse commercial electronics, such as multi-functional meter, calculator and RF-wireless temperature sensor. (g) The received temperature data from the RF-wireless temperature sensor.

To drive the common commercial electronics continuously for practical applications, two low-loss full-wave diode bridge rectifiers were integrated with an adjusting buck chopper to construct a complete energy managing circuit (EMC). The function of EMC is to regulate the pulse signal into a stable direct current (DC) signal (circuit diagram in Fig. 5d). Through integrating the H-P/TENG with the EMC, a complete DC power source was achieved to produce a stable and constant output voltage of 3.6 V (Fig. 5e). The common commercial electronics with different powers were successfully driven by the self-powered DC source. As illustrated in Fig. 5f (i), a multifunction meter without batteries was driven for a long time, the date and temperature could be clearly observed on the display screen (Video S3). A high-power consumption scientific calculator was also successfully driven to accomplish calculations by the self-powered DC source, as shown in Fig. 5f (ii) and Video S4. Besides, a more complicated radio-frequency (RF) wireless temperature transmission network, which included a temperature sensitive resistor, a radio-frequency (RF) transmitter, a microprocessor, and an AD module for converting analog into digital, could be readily driven by the self-powered DC source (Fig. 5f (iii) and **Video S5**). In the wireless transmission system, a RF receiver was utilized to collect and convert the temperature data from the wireless network into desired specific analog signals for data analysis. The RF transmitter emitted the digital signals that encoded the temperature information every two seconds. The self-powered DC source was suitable to power the intermittent signal acquisition and emission, indicating a self-powered real-time temperature monitor. The corresponding real-time temperature data was recorded in Fig. 5g. In addition, the proposed H-P/TENG was capable of harvesting various energies from the ambient environment (such as wind or air flow) by integrating with wind cups. We utilized a fan to perpendicularly blow on the wind cups and compel steady whirling of the rotor. At a wind speed of 14 m/s, the output voltage and current for the H-P/TENG were ~150 V and ~150 μA, respectively (Figure S7a and S7b). The scavenged wind energy could successfully light up 50 LEDs connected in parallel (Figure S7c and Video S6). Notably, all the applications are demonstrated at a low rotation speed of 100 rpm (equivalent to a frequency of 5 Hz), which is practical for harvesting the surrounding mechanical energy in low frequency. Meanwhile, as the output properties of the H-P/TENG are independent of the rotation speed (frequency), the H-P/TENG is capable of harvesting broadband mechanical energy stably and efficiently. It is promising to integrate the H-P/TENG with management circuits as a sustainable DC source for driving diverse commercial electronics. Furthermore, the proposed H-P/TENG works in a rotation mode, which can be readily integrated with other rotary type of triboelectric generators (*e.g.* rotary disk-based TENG and sleeve structured TENG) to deliver higher energy output.

Supplementary material related to this article can be found online at doi:10.1016/j.nanoen.2018.12.062.

## 3. Conclusion

In conclusion, we demonstrated a hybrid piezoelectric-triboelectric nanogenerator for stably/efficiently harvesting rotation mechanical energy to sustainably power various commercial electronics. According to the high performance bimorph-based PENG, the identical phase output and the matched impedances with TENG, the H-P/TENG could deliver high output voltage/current and large average power/power-density of ~210 V/395 μA and 10.88 mW/6.04 mW/cm$^2$, respectively. The high output performance was stable, appreciable and independent of rotation speed, which was promising for sustainably powering electronic devices by combining with suitable energy management circuits. The H-P/TENG was also capable of harvesting the wind energy to drive 50 LEDs. The simple structure of H-P/TENG exhibits large space to

integrate with other types of NG and ease for mass production. The proposed H-P/TENG is highly efficient and stable to harvest broadband bending or rotary mechanical energy, which has great potential for energy scavenging from surroundings (*e.g.* human motion, walk, bicycle, vehicle, motor wheel, wind, water flow, *etc.)* for the self-powered systems.

## 4. Experiments

### 4.1. Fabrication of the hybrid nanogenerator

To prepare the piezoelectric polymer in PENG, the P(VDF-TrFE) solution was prepared by dissolving P(VDF-TrFE) (70/30, molecular weight ~500,000) powder in *N*, *N*-Dimethylformamide solvent and stirred for 4 h at 25 ℃. The resulted uniform solution was cast on a clean glass and dried inside the oven (75 ℃) for 24 h to fully remove the solvent. Then the fabricated P(VDF-TrFE) film of 25 μm was annealed at 135 ℃ for 4 h to achieve the *β*-crystalline. Au electrodes were sputtered on both surfaces of the annealed film. The rectangular films (4 × 4.5 cm$^2$) were poled with DC electric field at 75 MV/m at 25 ℃ for 30 min to obtain high piezoelectricity through a high DC voltage source (ET2673A, Nanjing Entai electronic instruments plant, China). The unimorph or bimorph-based PENGs were prepared by mounting the poled one layer of P(VDF-TrFE) film or double layers of P(VDF-TrFE) films (25 μm) connected in parallel on a PET substrate (500 μm). For TENG, a thick aluminum tape was attached on a PET sheet of 125 μm as one of the friction layer. PTFE/Au was prepared on PET substrate as the other friction layer. ICP etching process (Sentech SI 500) was conducted for 2 min to manufacture nanostructure on the PTFE (80 μm) surface to enhance the triboelectrification effect. To fabricate the H-P/TENG, the bimorph-based PENG was attached on the opposite surface of PET substrate. The H-P/TENG was fixed on the upright post of the custom supporting frame as the stator. A shaft with three blades acted as the rotor to sweep through the H-P/TENG for scavenging rotary and flowing mechanical energy. A programmable motor was connected to the rotor to conduct the rotation process. The quantitative measurement of the electric output of the PENG, TENG and H-P/TENG. A function generator with power amplifier supply a driving signal for the shaker, which provided a vibration with different frequency and acceleration for the H-P/TENG cantilever beam without PET/Al layer. The acceleration was measured by an accelerator (121A01, YMC Piezoelectric Inc., Yangzhou, China).

### 4.2. Characterization of the materials and devices

The crystal phase of annealed P(VDF-TrFE) film was measured by Panalytical instrument (X′Pert 3 Powder). The surface morphology of etched PTFE and annealed P(VDF-TrFE) films was taken with SEM (Hitachi SU8020). The $V_{OC}$ and $I_{SC}$ of unimorph-based PENG, bimorph-based PENG, TENG and H-P/TENG were measured by oscilloscope (Tektronix Inc., Beaverton, OR, USA) and Keithley electrometer (6514A, Tektronix Inc., Beaverton, OR, USA). A variable resistor was connected with the rectified circuit to optimize the output power for PENG, TENG and H-T/PTENG.

## Appendix A. Supporting information

Supplementary data associated with this article can be found in the online version at doi:10.1016/j.nanoen.2018.12.062.

## References

[1] N.S. Lewis, Science 315 (2007) 798–801.
[2] Z.L. Wang, Sci. Am. 298 (2008) 82–87.
[3] M. Bariya, H.Y.Y. Nyein, A. Javey, Nat. Electron. 1 (2018) 160.
[4] Z.L. Wang, W.Z. Wu, Angew. Chem. Int. Ed. 51 (2012) 11700–11721.
[5] W. Gao, S. Emaminejad, H.Y.Y. Nyein, S. Challa, K. Chen, A. Peck, H.M. Fahad, H. Ota, H. Shiraki, D. Kiriya, D.-H. Lien, G.A. Brooks, R.W. Davis, A. Javey, Nature 529 (2016) 509.
[6] W. Gao, H.Y.Y. Nyein, Z. Shahpar, H.M. Fahad, K. Chen, S. Emaminejad, Y.J. Gao, L.-C. Tai, H. Ota, E. Wu, J. Bullock, Y.P. Zeng, D.-H. Lien, A. Javey, ACS Sens. 1 (2016) 866–874.
[7] A.A. Khan, M.H. Rehmani, A. Rachedi, IEEE Wirel. Commun. 24 (2017) 17–25.
[8] J. Chen, J. Yang, Z.L. Li, X. Fan, Y.L. Zi, Q.S. Jing, H.Y. Guo, Z. Wen, K.C. Pradel, S.M. Niu, Z.L. Wang, ACS Nano 9 (2015) 3324–3331.
[9] B.D. Chen, W. Tang, C. He, C.R. Deng, L.J. Yang, L.P. Zhu, J. Chen, J.J. Shao, L. Liu, Z.L. Wang, Mater. Today 21 (2018) 88–97.
[10] J.T. Zhang, Z. Fang, C. Shu, J. Zhang, Q. Zhang, C.D. Li, Sens. Actuators A 262 (2017) 123–129.
[11] J. Tollefson, Nature 508 (2014) 302.
[12] G.M.J. Herbert, S. Iniyan, E. Sreevalsan, S. Rajapandian, Renew. Sustain. Energy Rev. 11 (2007) 1117–1145.
[13] B. O'regan, M. Gratzel, Nature 353 (1991) 737.
[14] S. Xu, Y. Qin, C. Xu, Y.G. Wei, R.S. Yang, Z.L. Wang, Nat. Nanotechnol. 5 (2010) 366.
[15] Z.L. Wang, Adv. Mater. 24 (2012) 280–285.
[16] Z.L. Wang, Adv. Funct. Mater. 18 (2008) 3553–3567.
[17] Z.L. Wang, Faraday Discuss. 176 (2014) 447–458.
[18] K. Zhao, G.Q. Gu, Y.N. Zhang, B. Zhang, F. Yang, L. Zhao, M.L. Zheng, G. Cheng, Z.L. Du, Nano Energy 53 (2018) 898–905.
[19] G. Cheng, H.W. Zheng, F. Yang, L. Zhao, M.L. Zheng, J.J. Yang, H.F. Qin, Z.L. Du, Z.L. Wang, Nano Energy 44 (2018) 208–216.
[20] Y.L. Zi, H.Y. Guo, Z. Wen, M.-H. Yeh, C.G. Hu, Z.L. Wang, ACS Nano 10 (2016) 4797–4805.
[21] H. Kulah, K. Najafi, 17th IEEE International Conference on Micro Electro Mechanical Systems (MEMS), 2004,pp. 237–240.
[22] A.R.M. Foisal, G.S. Chung, J. Semicond. 33 (2012) 074001.
[23] H.Y. Guo, M.-H. Yeh, Y.-C. Lai, Y.L. Zi, C.S. Wu, Z. Wen, C.G. Hu, Z.L. Wang, ACS Nano 10 (2016) 10580–10588.
[24] X. Pu, L.X. Li, H.Q. Song, C.H. Du, Z.F. Zhao, C.Y. Jiang, G.Z. Cao, W.G. Hu, Z.L. Wang, Adv. Mater. 27 (2015) 2472–2478.
[25] T.Q. Trung, N.-E. Lee, Adv. Mater. 28 (2016) 4338–4372.
[26] L. Zheng, Z.-H. Lin, G. Cheng, W.Z. Wu, X.N. Wen, S.M. Lee, Z.L. Wang, Nano Energy 9 (2014) 291–300.
[27] X.Y. Du, N.W. Li, Y.B. Liu, J.N. Wang, Z.Q. Yuan, Y.Y. Yin, R. Cao, S.Y. Zhao, B. Wang, Z.L. Wang, C.J. Li, Nano Res. 11 (2018) 2862–2871.
[28] X.F. Wang, S.M. Niu, Y.J. Yin, F. Yi, Z. You, Z.L. Wang, Adv. Energy Mater. 5 (2015) 1501467.
[29] K.W. Zhang, X. Wang, Y. Yang, Z.L. Wang, ACS Nano 9 (2015) 3521–3529.
[30] R. Cao, T. Zhou, B. Wang, Y.Y. Yin, Z.Q. Yuan, C.J. Li, Z.L. Wang, ACS Nano 11 (2017) 8370–8378.
[31] H.F. Qin, G. Cheng, Y.L. Zi, G.Q. Gu, B. Zhang, W.Y. Shang, F. Yang, J.J. Yang, Z.L. Du, Z.L. Wang, Adv. Funct. Mater. (2018) 1805216.
[32] G. Cheng, Z.H. Lin, Z.L. Du, Z.L. Wang, Adv. Funct. Mater. 24 (2014) 2892–2898.
[33] J. Wang, C.S. Wu, Y.J. Dai, Z.H. Zhao, A. Wang, T.J. Zhang, Z.L. Wang, Nat. Commun. 8 (2017) 88.
[34] X. Pu, M.M. Liu, X.Y. Chen, J.M. Sun, C.H. Du, Y. Zhang, J.Y. Zhai, W.G. Huo, Z.L. Wang, Sci. Adv. 3 (2017) e1700015.
[35] Y. Yang, H.L. Zhang, X.D. Zhong, F. Yi, R.M. Yu, Y. Zhang, Z.L. Wang, ACS Appl. Mater. Interfaces 6 (2014) 3680–3688.
[36] J.J. Yang, F. Yang, L. Zhao, W.Y. Shang, H.F. Qin, S.J. Wang, X.H. Jiang, G. Cheng, Z.L. Du, Nano Energy 46 (2018) 220–228.
[37] G. Cheng, Z.H. Lin, L. Lin, Z.L. Du, Z.L. Wang, ACS Nano 7 (2013) 7383–7391.
[38] Y.L. Zi, L. Lin, J. Wang, S.H. Wang, J. Chen, X. Fan, P.-K. Yang, F. Yi, Z.L. Wang, Adv. Mater. 27 (2015) 2340–2347.
[39] Y.Q. Liu, N. Sun, J.W. Liu, Z. Wen, X.H. Sun, S.-T. Lee, B.Q. Sun, ACS Nano 12 (2018) 2893–2899.
[40] Z. Wen, H.Y. Guo, Y.L. Zi, M.-H. Yeh, X. Wang, J.N. Deng, J. Wang, S.M. Li, C.G. Hu, L.P. Zhu, Z.L. Wang, ACS Nano 10 (2016) 6526–6534.
[41] K.W. Zhang, S.H. Wang, Y. Yang, Adv. Energy Mater. 7 (2017) 1601852.
[42] W.-S. Jung, M.-G. Kang, H.G. Moon, S.-H. Baek, S.-J. Yoon, Z.L. Wang, S.-W. Kim, C.-Y. Kang, Sci. Rep. 5 (2015) 9309.
[43] S. Chen, X.M. Tao, W. Zeng, B. Yang, S.M. Shang, Adv. Energy Mater. 7 (2017) 1601569.
[44] M.D. Han, X.S. Zhang, B. Meng, W. Liu, W. Tang, X.M. Sun, W. Wang, H.X. Zhang, ACS Nano 7 (2013) 8554–8560.
[45] Q.M. Wang, X.H. Du, B.M. Xu, L.E. Cross, J. Appl. Phys. 85 (1999) 1702–1712.
[46] C.L. Zhao, J.X. Zhang, Z.L. Wang, K.L. Ren, Adv. Sustain. Syst. 1 (2017) 1700068.
[47] J.G. Wu, H.D. Shi, T.L. Zhao, Y. Yu, S.X. Dong, Adv. Funct. Mater. 26 (2016) 7186–7194.
[48] M.Y. Li, H.J. Wondergem, M.-J. Spijkman, K. Asadi, I. Katsouras, P.W.M. Blom, D.M.D. Leeuw, Nat. Mater. 12 (2013) 433.
[49] P. Martins, A.C. Lopes, S. Lanceros-Mendez, Prog. Polym. Sci. 39 (2014) 683–706.
[50] J. Chen, J. Yang, H.Y. Guo, Z.L. Li, L. Zheng, Y.J. Su, Z. Wen, X. Fan, Z.L. Wang, ACS Nano 9 (2015) 12334–12343.
[51] S.M. Niu, S.H. Wang, L. Lin, Y. Liu, Y.S. Zhou, Y.F. Hu, Z.L. Wang, Energy Environ. Sci. 12 (2013) 3576–3583.
[52] S.M. Niu, Z.L. Wang, Nano Energy 14 (2015) 161–192.
[53] Z.L. Wang, Mater. Today 20 (2017) 74–82.
[54] S.J. Jeong, M.S. Kim, J.S. Song, H.K. Lee, Sens. Actuators A 148 (2008) 158–167.

**Chunlin Zhao** received his B.S. degree from Harbin University of Science and Technology in 2013. Now he is a doctoral candidate in Beijing Institute of Nanoenergy and Nanosystems, Chinese Academy of Sciences. His research interests include self-charged energy package, piezoelectric functional material, semiconductors and their applications in self-powered sensor networks, human-machine interaction and energy harvester.

**Qian Zhang** received his B.S. degree from Hebei University of Technology in 2015. She obtained a master degree from Beijing Institute of Nanoenergy and Nanosystems, Chinese Academy of Science in 2018. She is now an Engineer in Second Research Institute of China Aerospace Science and Technology Group. Her research interests include piezoelectric functional material, electronic skin, graphene devices and their applications in self-powered sensor networks and human-machine interaction.

**Wenliang Zhang** received his B.S. degree from Shaanxi University of Science and Technology, China in 2015 and Master's Degreer from Shaanxi Normal University, China in 2017. He is now a research assistant in the Functional Soft Electronics Lab., Beijing Institute of Nanoenergy and Nanosystems (Chinese Academy of Sciences). His research interests focus on the fabrication of carbon-based electrode materials for energy storage and integration of micro-supercapacitors with triboelectric nanogenerators for self-charging power unit.

**Xinyu Du** received his Ph.D. from Beijing University of Technology in 2010. He worked as a postdoctoral researcher in International Center for Quantum Materials, Peking University. From 2015, he joined Beijing Institute of Nanoenergy and Nanosystems, Chinese Academy of Sciences. His research interests include Nanogenerators, nanosensors, nanodevices and scattering spectrum study of materials with strong electron correlations.

**Dr. Yang Zhang** received his M.S. (2009) from Beijing Normal University and Ph.D. (2013) from the Leibniz Institute for Solid State and Materials Research Dresden. Currently, he is an Assistant Professor at Beijing Institute of Nanoenergy and Nanosystems, Chinese Academy of Sciences. His research focuses on the novel nanocomposites and their applications in energy harvesting, photoelectric nanodevice, photocatalyst and electrocatalyst.
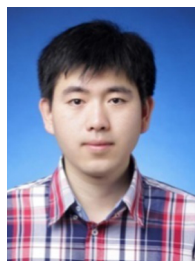
**Prof. Qijun Sun** received his Ph.D. from Gachon University in 2013. After that, he worked as a postdoctoral researcher in POSTECH (2013) and SKKU (2014). In 2015, he worked in Sungkyunkwan University as a research professor. From 2016, he joined Beijing Institute of Nanoenergy and Nanosystems (Chinese Academy of Sciences), as the principal investigator of Functional Soft Electronics Lab. The Main research interests of his group include graphene device based E-skin, organic electronic device, graphene electronics, printing electronics, micro-nano fabrication and transparent conducting films, aim to develop advanced systems for human health monitoring and human-machine interface.
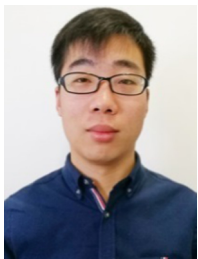
**Shaobo Gong** received his B.S. degree from Hebei University of Technology in 2015. Now he is a doctoral candidate in Beijing Institute of Nanoenergy and Nanosystems, Chinese Academy of Sciences. His research interests include electret, piezoelectric functional material and their applications in self-powered sensor networks, flexible electronic skin and energy harvester.

**Prof. Zhong Lin Wang** received his Ph.D. from Arizona State University in physics. He now is the Hightower Chair in Materials Science and Engineering, Regents' Professor, Engineering Distinguished Professor and Director, Center for Nanostructure Characterization, at Georgia Tech. Prof. Wang has made original and innovative contributions to the synthesis, discovery, characterization and understanding of fundamental physical properties of oxide nanobelts and nanowires, as well as applications of nanowires in energy sciences, electronics, optoelectronics and biological science. His discovery and breakthroughs in developing nanogenerators established the principle and technological roadmap for harvesting mechanical energy from the environment and biological systems for powering a personal electronics. His research on self-powered nanosystems has inspired the worldwide effort in academia and industry for studying energy for micro-nano-systems, which is now a distinct disciplinary in energy research and future sensor networks. He coined and pioneered the field of piezotronics and piezophototronics by introducing piezoelectric potential gated charge transport process in fabricating new electronic and optoelectronic devices. Details can be found at: www. nanoscience.gatech.edu

**Kailiang Ren**, Ph.D., professor. He obtained his M.S. and Ph.D. degree from the Pennsylvania State University in 2005 and 2007, respectively. He was a postdoctoral fellow at the Pennsylvania State University from 2009 to 2010 and Johns Hopkins University from 2011 to 2014. Currently, he is a professor at Beijing Institute of Nanoenergy and Nanosystems. His primary research interests focus on device applications of novel electronic materials, especially soft electronic materials and ferroelectric-based materials, which include piezoelectric nanofiber based nanogenerators, energy devices for electrical energy storage and conversion, and MEMs sensors. He has authored and co-authored over 30 *publications,* one US patent and 2 patents pending.